Functional Evaluation of Serine/Threonine Residues in the P-Loop of *Rhodobacter sphaeroides* Phosphoribulokinase†

Jennifer A. Runquist, Sandra E. Ríos, Dmitriy A. Vinarov, and Henry M. Miziorko*

Department of Biochemistry, Medical College of Wisconsin, Milwaukee, Wisconsin 53226

Received April 17, 2001; Revised Manuscript Received October 2, 2001

ABSTRACT: The N-terminal region of phosphoribulokinase (PRK) has been proposed to contain a "P-loop" or "Walker A" motif. In *Rhodobacter sphaeroides* PRK, four alcohol side chains, contributed by S14, T18, S19, and T20, map within the P loop and represent potential Mg−ATP ligands. Each of these has been individually replaced with an alanine and the impact of these substitutions on enzyme−ATP interactions and overall catalytic efficiency evaluated. Each mutant PRK retains the ability to tightly bind the positive effector, NADH (0.7−0.9 per site), and exhibits allosteric activation, suggesting that the proteins retain a high degree of structural integrity. Similarly, each mutant PRK retains the ability to stoichiometrically (0.7−1.2 per site) bind the alternative substrate trinitrophenyl-ATP. Despite the large size of the PRK oligomer (8 × 32 kDa), ^{31}P NMR can be used to detect stoichiometrically bound Mg−ATP substrate, which produces markedly broadened peaks in comparison with signals from unbound Mg−ATP. Elimination of alcohol substituents in mutants T18A, S19A, or T20A produces enzymes which retain the ability to form stable PRK∗Mg−ATP complexes. Each mutant complex is characterized by ^{31}P resonances for α- and γ-phosphoryls of bound Mg−ATP which are narrower than measured for wild-type PRK∗Mg-ATP; signals for the β-phosphoryl are poorly detectable for mutant PRK∗Mg-ATP complexes. Kinetic characterization indicates that these mutants differ markedly with respect to catalytic activity. T20A exhibits V_m comparable to wild-type PRK, while V_m is diminished by 8-fold for T18A and by 40-fold for S14A. In contrast to these modest effects, S19A exhibits decreases in V_m and V_m/K_{Ru5P} of 500-fold and >15000-fold, respectively. S19A and T18A exhibit only modest (6−7-fold) increases in $S_{1/2}$ for ATP but larger (30−45-fold) increases in K_m for Ru5P. K_I values for the competitive inhibitor, 6-phosphogluconate, do not significantly change upon mutation of T18 or S19, suggesting that these residues are not crucial to Ru5P binding. A role for the alcohol group of S19, the eighth residue in P-loop motif, as a ligand to the Mg−ATP substrate seems compatible with the characterization data; adjacent alcohols do not efficiently function as surrogates. Such a proposed function for S19 is compatible with its proximity to E131, the acidic residue in a putative Walker B motif and probable second Mg−ATP ligand in PRK's active site.

Phosphoribulokinase (PRK;[1] EC 2.7.1.19) catalyzes transfer of the γ-phosphoryl of ATP to the C1 hydroxyl of ribulose 5-phosphate (Ru5P) to form ribulose 1,5-bisphosphate (*1*), the CO_2 acceptor of the reductive pentose phosphate pathway. Since this reaction is a key step in CO_2 assimilation, PRK has been identified in a variety of plants, algae, and bacteria that rely on such metabolism. Eukaryotic and prokaryotic PRKs differ significantly; sequence alignments suggest that only ∼13% of total amino acids in PRKs are strictly invariant (*2*). Despite these contrasts, the clustering of invariant residues in regions that define the active site or form the critical subunit−subunit interface (*3*) suggests that PRKs from these diverse sources are likely to be structurally homologous.

High-resolution structures of *Rhodobacter sphaeroides* PRK have been reported (*3*, *4*). While the crystallized protein contains no metabolites bound at the active site, mutagenesis work has implicated residues involved in Ru5P binding (*5*, *6*). PRK's fold places it in the structurally well-characterized nucleotide monophosphate (NMP) kinase family of proteins. Recognition of a consensus nucleotide binding site for this family of proteins allowed our provisional assignment of the binding site in PRK for the phosphoryl donor substrate, ATP. More specifically, the N-terminal region of PRK includes a "Walker A" or "P-loop" motif (*7*, *8*). The observation that this PRK loop is situated in the region of the NMP kinase fold proposed as the consensus ATP binding site supports our tentative assignment. Much of the functional testing of this region has focused on its importance in regulation of the eukaryotic enzyme (*9*, *10*). However, the demonstrated ability of ATP to protect PRK from covalent modification of this region (*11*−*13*) represents an experimental test that supports the mapping of the P-loop region as part of PRK's active site. Unfortunately, this loop exhibits very dynamic motion, even in crystalline PRK, and the high-resolution

† This work was supported in part by grants from the USDA (NRI-CRG Photosynthesis) and the DOE (DE-FG02-OOER15100).

* To whom correspondence should be addressed. Telephone: 414-456-8437. Fax: 414-456-6570. E-mail: miziorko@mcw.edu.

[1] Abbreviations: PRK, phosphoribulokinase; Ru5P, ribulose 5-phosphate; RuBP, ribulose 1,5-bisphosphate; TNP-ATP, 2′(3′)-*O*-(2,4,6-trinitrophenyl)adenosine 5′-triphosphate; IPTG, isopropyl thiogalactoside; 6PG, 6-phosphogluconate; T_2, transverse relaxation time.

10.1021/bi010778c CCC: $20.00
Published on Web 11/08/2001

structure (*3*) exhibits a main chain break in this region. Thus, specific residues directly involved in ATP binding remain to be firmly established.

One plausible approach for identification of ATP binding residues involves detection of the amino acids that ligand to the cation of the $M^{2+}-$ATP substrate. In the case of NMP kinase fold proteins, no absolute consensus regarding cation ligation has been established. For example, amino acid ligands to the cation of the $M^{2+}-$ATP substrate have been implicated for some enzymes (*14*, *15*) which exhibit NMP kinase folds while other enzymes in this family (*16*, *17*) do not utilize amino acids as cation ligands. The possibility that one of the multiple alcohol side chains in PRK's dynamic P-loop interacts with $M^{2+}-$ATP is addressed in this report. A preliminary account of these studies has appeared (*18*).

MATERIALS AND METHODS

Materials. Deoxyoligonucleotides and fluorescein-labeled sequencing primers were purchased from Operon Technologies, Inc. PCR generation of DNA pieces utilized Stratagene's *Pfu* DNA polymerase. T4 DNA ligase and restriction enzymes were obtained from New England Biolabs. Isolation of plasmid DNA, grown in competent *Escherichia coli* JM109(Promega), was accomplished using Sigma's plasmid pure miniprep kit, and Qiagen's plasmid mini and midi kits. Isolation of DNA fragments was accomplished using a QIAEX II gel extraction kit. DNA sequence analysis was performed using a Thermo sequenase core sequencing kit from Pharmacia/Amersham Life Sciences and a Pharmacia/LKB ALF DNA sequencer.

For recombinant protein expression, ampicillin was purchased from Fisher Scientific, isopropyl β-D-thiogalactoside (IPTG) from Research Products International Corp., and competent *E. coli* BL21(DE3) cells from Novagen. Adenosine 5′-triphosphate, D-ribulose 5-phosphate, DTT, Hepes, and Tris-HCl buffers were obtained from Sigma Chemical Co. Sodium [^{14}C]bicarbonate, 56 mCi/mmol, was a product of American Radiolabeled Chemicals, Inc. Chromatography media utilized for PRK isolation included reactive green-19 agarose from Sigma Chemical Co. and Q-Sepharose fast flow from Pharmacia Biotech. For fluorescence experiments, TNP-ATP [2′(3′)-*O*-(2,4,6-trinitrophenyl)adenosine 5′-triphosphate] from Molecular Probes was monitored. The RuBP carboxylase required for the CO_2 fixation assay of PRK activity was isolated after expression in *E. coli* JM103 using a plasmid generously provided by C. R. Somerville.

Construction of prkA Mutant Alleles. Mutagenesis of the P-loop residues with single amino acid substitutions, S14A, T18A, S19A, and T20A, was accomplished using pETbprkwt. Four 450 bp pieces with the appropriate mutations were generated using PCR overlap extension. For S14A, TCC was mutated to GCC; for T18A, ACC was mutated to GCC; for S19A, TCG was mutated to GCG; for T20A, ACG was mutated to GCG. The purified mutated DNA samples were cut with *Nco*I and *Sac*I and the resulting fragments ligated in a three-way ligation strategy, previously reported, to generate pETbprkS14A, pETbprkT18A, pETbprkS19A, and pETbprkT20A, respectively. Plasmids potentially encoding the desired mutants were screened to verify that the appropriate restriction enzyme sites were still intact. DNA sequencing confirmed that the selected expression plasmids encoded the anticipated alanine substitutions and verified that no addition mutations had been introduced during PCR overlap extension.

Expression and Purification of PRK. *E. coli* BL21(DE3) cultures containing plasmids pETbprkS14A, pETbprkT18A, pETbprkS19A, and pETbprkT20A were grown at 25 °C in 2 L of ampicillin-containing LB media to an OD_{600} of ~0.5. Expression of PRK was induced by addition of IPTG to a final concentration of 1 mM followed by 3−4 h of additional growth. The cells were collected by low-speed centrifugation; cell pellets were suspended and disrupted using a French pressure cell. A 100000*g* supernatant was prepared and subjected to Q-Sepharose anion-exchange chromatography followed by affinity chromatography on reactive green-19 agarose. PRK was eluted from reactive green-19 agarose affinity resin with a buffer containing 25 mM Tris-HCl (pH 8.2), 10 mM mercaptoethanol, 1 mM EDTA, and 10 mM ATP. ATP removal from ATP eluted enzyme was accomplished by prolonged dialysis. For quantitative protein concentration estimates, an extinction coefficient of 50303 M^{-1} cm^{-1} at 280 nm was used (*19*).

TNP-ATP and NADH Binding Stoichiometry Measurements. TNP-ATP binding to PRK was evaluated by fluorescence measurements on a SLM 4800C spectrofluorometer as described previously (*19*). Relative fluorescence was measured at the fluorescence emission peak of 545 nm for PRK-bound TNP-ATP. NADH binding to PRK was also measured using fluorescence methods. In this case, fluorescence was measured at the emission peak of 440 nm for PRK-bound NADH. The binding stoichiometry of mono- and dinucleotides to PRK was determined from the intersection point of lines fit to the substoichiometric and plateau regions of the titration data by linear regression (*20*, *21*). Calculated stoichiometries reflect binding sites per 32 kDa PRK.

Kinetic Characterization of PRK. A radioisotopic assay that involves trapping the PRK reaction product RuBP via the RuBP carboxylase-dependent incorporation of $^{14}CO_2$ to form acid-stable [^{14}C]-3-phosphoglycerate (*22*) was utilized. In standard assays, the final concentrations of reaction mixture components were 100 mM Hepes, pH 8.0, 1 mM DTT, 20 mM $MgCl_2$, 20 mM $KH^{14}CO_3$ (~1000 dpm/nmol), 5 mM ATP, 1 mM Ru5P, 1 mM NADH, and 100 milliunits of recombinant RuBP carboxylase. Enzyme assays were conducted at 30 °C. For kinetic characterization of the mutant proteins, ATP concentration ranges varied from 0.05 to 15 mM; Ru5P concentration ranges varied from 0.05 to 8 mM. Kinetic data were fit by a nonlinear regression analysis algorithm (*23*).

EPR and ^{31}P NMR Measurements of PRK∗$M^{2+}-$ATP Complexes. Since the protein is isolated by an ATP elution from reactive green 19, removal of excess ATP from the enzyme preparation is required. In the absence of divalent cation, even after centrifugal gel filtration or after prolonged dialysis (24 h) ATP can remain tightly bound to both the catalytic site and the allosteric nucleotide (NADH/AMP) binding site. To achieve selective ATP binding, protein is supplemented with a divalent cation (e.g., Mg^{2+}, Mn^{2+}) prior to removal of excess ATP. This approach produces samples containing $M^{2+}-$ATP bound only at the active site; the allosteric site becomes vacant and is available for titration with effector nucleotides (*19*).

For the smaller amounts of protein needed for EPR, PRK (35 uM) was dialyzed to lower excess ATP levels and then incubated with Mn^{2+} (1 mM) and ATP (0.3 mM). Excess cation and nucleotide were then removed by centrifugal gel filtration using G-50 columns; samples (ATP/PRK ~1:1) were concentrated to 200−300 μM enzyme sites. EPR measurements were performed at 22 °C using a Varian E-109 spectrometer.

For the larger amounts of protein complex needed for ^{31}P NMR studies, the enzyme was diluted to about 3−4 mg/mL (4−6 mL) and dialyzed against 50 mM Tris-HCl, pH 8.0, 0.2 mM EDTA, and 5 mM $MgCl_2$. Several days of dialysis were required to achieve a nucleotide/PRK ratio of ≤1.0. The ATP/PRK stoichiometry was determined from the 260/280 nm ratio (*19*). Estimates of ATP binding stoichiometry are based on a calibration curve that ranges from a 260/280 ratio of 0.67 for no ATP bound to a 260/280 value of 0.97 for 1 ATP bound per 32 kDa PRK subunit (*19*). Concentration of PRK∗M^{2+}−ATP was accomplished using either an Amicon Centricon 10 or a 4 mL centrifugal filter and tube device from Millipore with a 10K NMWL (nominal molecular weight limit). For ^{31}P NMR, a final sample volume of 0.46 mL with protein concentrations ranging from 0.35 to 0.85 mM was employed; sample volume was brought to 0.5 mL with D_2O to provide a lock signal. Samples were treated with Chelex (resin removed by filtration using a 0.2 μm Lida microspin filter; Chrom Tech) to eliminate potential paramagnetic metal contaminants. Final protein concentrations and ATP binding stoichiometries were determined from 280 and 260/280 nm determinations, respectively.

NMR measurements were performed on a Bruker AC 300 using a 5 mm multinuclear QNP probe operating at 121.5 MHz for ^{31}P. Spectra of PRK-bound ATP were measured at 21 °C. Broad-band proton decoupling was used in acquiring all spectra. Signal acquisition was performed using the following experimental parameters: spectral width, 10000 Hz; line broadening, 20 Hz for protein samples (5 Hz for free nucleotide samples); acquisition delay, 5 s; pulse angle, 35°; number of transients, 4500 for protein samples (400 for free nucleotide samples). Spectra displayed in the figure were zero-filled to 64K to improve the signal to noise ratio.

RESULTS

Strategy for Identification of an Active Site M^{2+}−ATP Ligand: *Mutagenic Substitution of Alcohol Side Chains in P-Loop Residues.* In those phosphotransferases that use two amino acid side chains to bind the cation of the M^{2+}−ATP substrate, usually two acidic residues or one acidic amino acid and one serine/threonine are functionally involved (*24*). In the case of PRK, each of the four invariant acidic residues (D42, E131, D169, E178) has been functionally evaluated by mutagenesis and kinetic characterization approaches (*25*). Replacement of E178 has no substantial impact on catalytic efficiency. In contrast, elimination of the side chain carboxyl group of E131, D169, or D42 results in a diminution of activity by 2, 4, or 5 orders of magnitude, respectively. Mutagenesis of D169 and D42 results in effects that are larger than might be expected for elimination of a group that functions solely to provide one ligand to the cation. In contrast, such a functional assignment agrees well with the consequences of mutating E131(100-fold diminution in catalytic efficiency). Since only one acidic residue emerges as a good cation ligand candidate, the possibility that an alcohol functions as the probable second ligand seems attractive. There are only two invariant PRK residues with alcohol side chains, S14 and T214. The latter residue is positioned at the subunit interface that defines the evolutionarily conserved dimer (*4*); this region is well removed from the catalytic site, and therefore, T214 can be discounted as a cation ligand. The other residue, S14, is situated within a P-loop, which is well precedented to interact with ATP. In the case of *R. sphaeroides* PRK, this loop also contains three other residues (Figure 1) with alcohol side chains, namely, T18, S19, and T20. While S14 is strictly invariant, a serine or threonine is always represented at PRK residues 19 and 20. An alcohol side chain is present at position 18 only in prokaryotic PRKs. On the basis of these observations, site-directed mutagenesis was performed to eliminate the alcohol side chain at each of these four positions (S14, T18, S19, and T20) in *R. sphaeroides* PRK. We anticipated not only that characterization of these mutants would lead to functional identification of a cation ligand but also that the ability of an adjacent alcohol side chain in this mobile loop to function as a surrogate cation ligand might be tested.

```
                      10         20
      arabprk    .AQETIVIGL AADSGCGKST FMRR
       whtprk    AVEQPIVIGL AADSGCGKST FMRR
     mescrprk    GDSQTIVIGL AADSGCGKST FMRR
       spprk     SQQQTIVIGL AADSGCGKST FMRR
        cprk     DKDKTVVIGL AADSGCGKST FMRR
      sycprk     QLDRVVLIGV AGDSGCGKST FLRR
       rsprk     MSKKHPIISV TGSSGAGTST VKHT
       aeprk     MSERYPIIAI TGSSGAGTTS VTRT
     nitroprk    VLRKHPIISI TGSSGAGTTS VKRT
   xflavusprk    MSIKHPIIVV TGSSGAGTTS VKRT

     WALKER A                GXXGXGKT/S
```

FIGURE 1: Alignment of deduced PRK sequences to indicate homology in the N-terminal region. Ten representative eukaryotic or prokaryotic sequences are shown, corresponding to PRKs from *Arabidopsis*, wheat, ice plant, spinach, *Chlamydomonas*, *Synechocystis*, *R. sphaeroides*, *Alcaligenes eutrophus*, *Nitrobacter vulgaris*, and *Xanthobacter flavus*. Residue numbering corresponds to the *R. sphaeroides* enzyme. Below appears the consensus Walker A or P-loop sequence.

Overlap extension PCR (*26*) was used to replace each alcohol-containing residue with alanine. Expression of the mutant-encoding plasmids produced stable proteins which behaved similarly to the wild-type protein upon purification; they were recovered in a highly homogeneous form and at yields comparable to the wild-type enzyme. Each purified mutant PRK exhibits a single major band on SDS−PAGE, migrating similarly to the 32 kDa wild-type protein (Figure 2). The enzymes exhibited good stability during the biophysical and kinetic characterization experiments described below.

Biophysical Characterization of PRK Mutants. To ensure that the mutant PRKs retain substantial structural integrity (and are, therefore, useful for detailed characterization), ligand binding at the catalytic and effector sites was evaluated. The fluorescent ATP analogue, TNP-ATP, is an alternative substrate for PRK and titrates wild-type enzyme to stoichiometrically form a stable binary complex (*19*). The ability of mutant PRKs to bind this analogue has been tested (Figure 3); fluorescence titrations indicate no substantial differences in binary complex formation (Table 1), suggesting

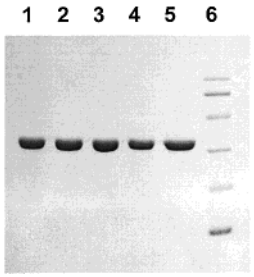

FIGURE 2: SDS−PAGE of wild-type and mutant *R. sphaeroides* PRKs. Lanes 1−5 contain wild-type PRK, PRK-S14A, PRK-T18A, PRK-S19A, and PRK-T20A, respectively. Lane 6 contains molecular mass markers (phosphorylase, 97.4 kDa; bovine serum albumin, 66.2 kDa; ovalbumin, 45 kDa; carbonic anhydrase, 31 kDa; trypsin inhibitor, 21.5 kDa; and lysozyme, 14.4 kDa).

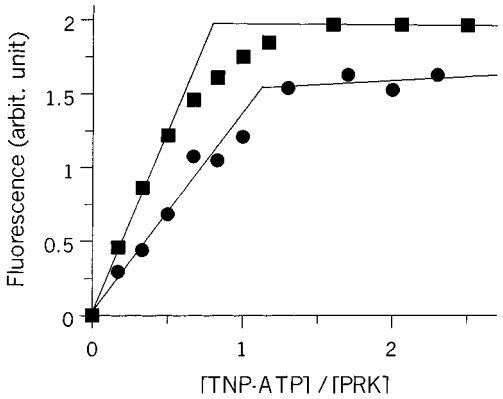

FIGURE 3: Fluorescence titration of PRK-S19A by TNP-ATP. Sequential additions of TNP-ATP were made to a fluorescence cuvette containing 5.4 μM wild-type (■) or 6.0 μM S19A (●) PRK proteins (previously stripped of ATP by exhaustive dialysis) in 25 mM Tris-HCl, pH 8.0. The relative fluorescence enhancement is plotted versus the ratio of added TNP-ATP per enzyme site. Binding stoichiometry is estimated from the intersection point of lines fit to the low- and high-occupancy data points by linear regression analyses.

Table 1: Substrate and Effector Binding by PRK Mutants[a]

enzyme	n_{NADH}	$n_{TNP-ATP}$
wild type	0.77 ± 0.03	0.81 ± 0.03
S14A	0.92 ± 0.09	1.23 ± 0.05
T18A	0.68 ± 0.04	0.73 ± 0.10
S19A	0.67 ± 0.02	1.10 ± 0.08
T20A	0.81 ± 0.04	1.00 ± 0.09

[a] *n* denotes the calculated number of binding sites per enzyme subunit. Stoichiometries for TNP-ATP and NADH binding were determined from fluorescence titrations.

that the active sites of these mutants retain a high degree of structural integrity. Likewise, the overall structural integrity of PRK can be tested by probing with the fluorescent allosteric activator, NADH. Titrations with NADH demonstrate effector site binding stoichiometries that closely approach the value measured for wild-type PRK (Table 1). These observations suggest that both the active site and effector site of each mutant are intact, and therefore, it follows that the overall tertiary structure of each of these PRK mutants closely resembles that of the wild-type enzyme. Thus, any substantial differences in catalytic efficiency or other kinetic parameters that may be exhibited by these PRK mutants can be interpreted in a reasonably straightforward fashion since, by the resolution of the physical characterization experiments, there is no gross structural perturbation of any of the mutant enzymes.

The possibility that a biophysical approach might provide direct evidence of interaction between PRK amino acids and M^{2+}−ATP has also been addressed. Earlier work (*19*) has documented PRK's ability to form very stable binary PRK∗M^{2+}−ATP complexes[2] in which nucleotide occupies the catalytic site [as well as ternary complexes which contain nucleotides bound in both M^{2+}−ATP substrate and allosteric effector (NADH/AMP) sites]. By using Mn^{2+} to produce the stable binary complex in which M^{2+}−ATP occupies the substrate site, a sample that allows observation of this paramagnetic cation by EPR is generated. Such an approach could facilitate comparison of wild-type PRK and P-loop mutants if active site liganding changes for the mutants were manifest as detectable spectral changes. However, the 9 GHz EPR spectra of protein-bound Mn^{2+} vary widely in appearance, depending on whether and how the normally cubic ligand field of the cation is distorted upon binding to protein and/or metabolite ligands. In some cases, partial resolution of normally degenerate fine structure transitions can be detected (*27*), but in other cases (*28*), spectral features are broadened and/or superimposed, making detailed interpretation of the Mn^{2+}−protein complex spectrum difficult. The EPR spectrum of PRK∗Mn^{2+}−ATP falls into the latter category (Figure 4A), exhibiting poorly resolved features. No significant difference in spectral features is detected upon comparison of spectra measured for complexes prepared using wild-type or P-loop mutant PRKs (Figure 4B). Even after several days at ambient temperature, no substantial changes in EPR spectra are observable (e.g., no free Mn^{2+} signal appears), suggesting that dissociation of the model complex is a very slow process. On the basis of the possibility that diamagnetic probes such as Mg^{2+} or Mg^{2+}−ATP might competitively displace Mn^{2+} in a fashion that would allow discrimination between wild-type and P-loop mutant PRKs, samples were challenged by incubation with either Mg^{2+} (>40-fold excess) or Mg^{2+}−ATP (>8-fold excess) and monitored for the possible displacement of unbound Mn^{2+}, detectable as a pattern of six narrow lines. Regardless of whether wild-type or P-loop mutant PRKs were used for production of the PRK∗Mn^{2+}−ATP samples, no free Mn^{2+} could be detected even after >20 h of incubation with excess Mg^{2+} or Mg^{2+}−ATP. The complexes are sufficiently stable that only after denaturation by prolonged incubation with SDS is the six-line spectrum of free Mn^{2+} detectable (Figure 4C,D). Thus, while the EPR data suggest that the P-loop mutants retain substantial structural integrity, based on their formation of stable complexes that are similar to those produced with wild-type enzyme, the direct cation observation approach does not discriminate between functional importance of P-loop residues. This outcome prompted evaluation of the utility of a different biophysical approach.

Despite the large size of the native PRK octamer (~250 kDa), an attempt was made to detect this complex by ^{31}P NMR. Mg^{2+}−ATP bound to native PRK produces a spec-

[2] In a strict sense, the model PRK∗M^{2+}−ATP complex may represent an equilibrium complex. However, the slow half-life (several days) for dissociation of PRK∗M^{2+}−ATP after this species is isolated free of excess M^{2+}−ATP indicates that the biophysical experiments reported in this paper are performed using a very slowly exchanging complex.

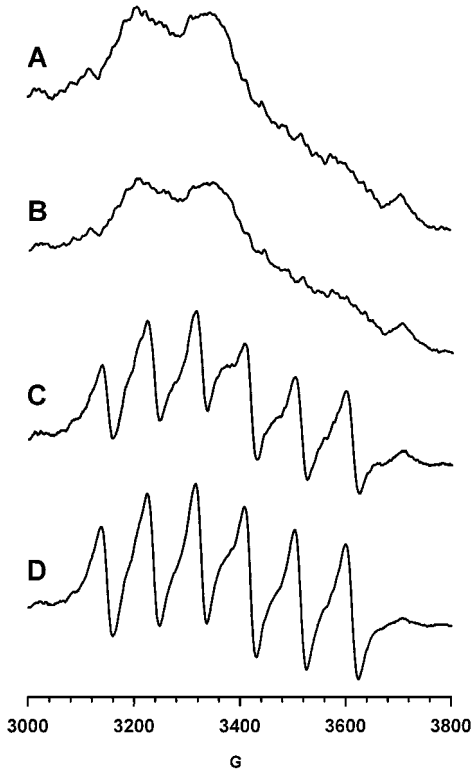

FIGURE 4: EPR spectrum of PRK∗Mn^{2+}−ATP complexes. (A) The spectrum of a native complex (298 μM) is displayed; it was acquired by accumulation/averaging of 12 scans (4 min for each scan). (B) The spectrum of a comparable sample (286 μM), prepared using S19A PRK (14 scans averaged) is displayed. Instrument settings were microwave frequency, 9.415 GHz; microwave power, 50 mW; modulation amplitude, 10 G; modulation frequency, 100 kHz; gain, 2.5×10^3; scan range, 1000 G; and time constant, 0.25 s. Measurements were performed at 22 °C. For spectra C and D, samples equivalent to those used for spectra A and B were brought to 1% SDS, heated for 5 min at 70 °C, and subsequently incubated for 24 h at ambient temperature. The spectra were measured on the resulting denatured samples [268 μM for denatured wild type (spectrum C); 266 μM for denatured S19A (spectrum D)] using the same instrumental conditions as described above, except that 15 scans (4 min for each scan) were accumulated/averaged for each trace.

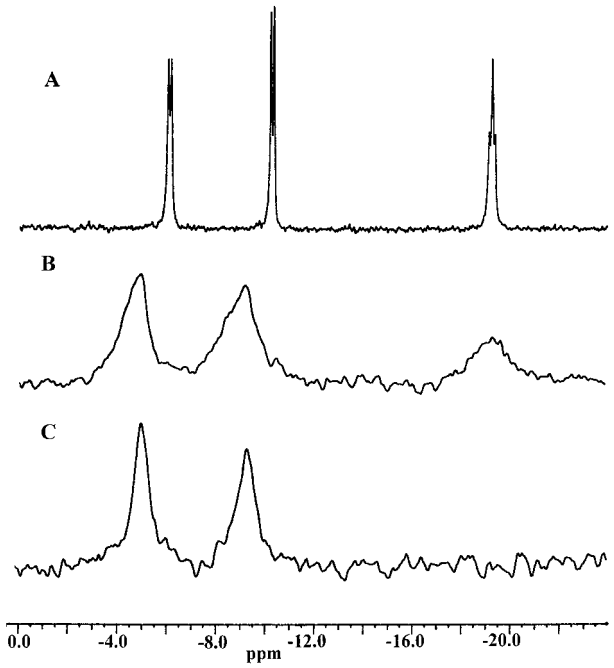

FIGURE 5: ^{31}P spectra of free and PRK-bound Mg^{2+}−ATP. In (A), the spectrum was measured using a 1.0 mM sample of Mg^{2+}−ATP in 10 mM Tris-HCl, pH 8.0. In (B) and (C), spectra were measured on samples containing ~0.9 tightly bound (nonexchangeable) Mg^{2+}−ATP per PRK site. Protein concentrations in both sample B (wild-type PRK) and sample C (S19A) were 0.7 mM. Spectra were acquired for 0.5 h (A) or 6 h (B, C) at 21 °C under conditions described in Materials and Methods.

Table 2: ^{31}P NMR Spectral Parameters for Free and PRK-Bound Mg^{2+}−ATP[a]

	δ, ppm			line width, Hz		
sample	α	β	γ	α	β	γ
Mg^{2+}−ATP	−10.3	−19.2	−6.1	7[b]	12[b]	9[b]
wt PRK∗Mg^{2+}−ATP	−9.3	−19.4	−5.0	193	230	145
PRK-T18A∗Mg^{2+}−ATP	−9.3	nd[c]	−5.0	106	nd	91
PRK-S19A∗Mg^{2+}−ATP	−9.3	nd	−5.0	109	nd	85
PRK-T20A∗Mg^{2+}−ATP	−9.3	nd	−5.0	99	nd	91

[a] Enzyme samples (0.35−0.85 mM) contained 0.9 ATP per PRK site. Spectral acquisitions were performed on a Bruker AC-300 using a 5 mm QNP multinuclear probe operating at 121.5 MHz for ^{31}P. Acquisition parameters are specified in Materials and Methods. Error in chemical shift measurements is <0.05 ppm. [b] Line widths for peaks of free Mg^{2+}-ATP are reported as width at half-height for one line of the doublet signals observed for α− and γ-phosphoryl groups and for the middle peak of the β-phosphoryl triplet. Typical error is <5 Hz. [c] Chemical shifts and line widths for the β-phosphoryl signals are not detectable in samples prepared using the T18A, S19A, and T20A mutants.

trum in which each phosphoryl group can be detected (Figure 5), although these signals exhibit significant broadening (145−230 Hz; Table 2) in comparison with the corresponding signals observed for Mg^{2+}−ATP in buffer. Additionally, the peaks corresponding to the α- and γ-phosphoryl resonances are each shifted downfield by approximately 1 ppm. As pointed out by Brauer and Sykes (*29*), changes in ^{31}P shifts upon binding of ligands to proteins may reflect multiple contributions, and predictable patterns are not always apparent. In contrast, binding of a phosphorus-containing ligand to a protein will usually decrease the transverse relaxation time (T_2) due to immobilization of the ^{31}P nucleus, producing an observable line broadening of the type depicted in Figure 5B. On the basis of the observation of substantial line broadening upon wild-type PRK binding of Mg^{2+}−ATP, the ^{31}P NMR approach was extended to study the T18A, S19A, and T20A mutant PRKs. Just as in the case of TNP-ATP, all three of these mutant PRKs mimic the wild-type enzyme by forming stable binary complexes with Mg^{2+}−ATP. This allowed NMR observation of the bound nucleotide (which is certainly in slow exchange on an NMR time scale). Interestingly, the signal due to the β-phosphoryl group was not reliably detectable in complexes prepared using the mutant PRKs (Figure 5C). In contrast, the signals attributable to α- and γ-phosphoryls were easily measurable since, in the case of each of the three mutants (T18A, S19A, and T20A) that were used for this type of experiment, the signals attributable to α- and γ-phosphoryls were narrower in line width than signals for the complex formed using the wild-type enzyme (Table 2). It is possible that this signal narrowing reflects less efficient transverse (T_2) relaxation due to decreased immobilization of the α- and γ-phosphoryl groups in the complexes formed using the P-loop mutants. Alteration of binding interactions between PRK and Mg^{2+}−

Table 3: Steady-State Kinetic Parameters of Wild-Type and Mutant PRKs[a]

enzyme	$K_{m\ RU5P}$ (mM)	n_H	$K_{I\ 6PG}$ (mM)	$S_{1/2\ ATP}$ (mM)	n_H	V_{max} (units/mg)	NADH activation (*x*-fold)
WT	0.096 ± 0.014	h	0.22[b] ± 0.02	0.55 ± 0.16	1.98 ± 0.15	338 ± 18.0	≃40
S14A	0.586 ± 0.098	h	nd[c]	0.99 ± 0.09	1.57 ± 0.12	8.10 ± 0.49	≃20
T18A	4.50 ± 1.16	h	0.20 ± 0.03	4.00 ± 0.03	2.61 ± 0.22	44.4 ± 5.9	≃40
S19A	3.16 ± 0.18	1.54 ± 0.11	0.22 ± 0.05	3.41 ± 0.11	2.10 ± 0.46	0.70 ± 0.04	≃40
T20A	0.662 ± 0.058	h	nd[c]	1.13 ± 0.10	1.42 ± 0.25	320 ± 40	≃40

[a] The $K_{m\ Ru5P}$ is the ribulose 5-phosphate concentration at half-maximal velocity, as calculated from a fit of the Ru5P saturation data to the Michaelis−Menten equation. The $S_{1/2\ ATP}$ is the ATP concentration at half-maximal velocity, as calculated from a fit of the ATP saturation data to the Hill equation. n_H is the Hill constant. h indicates that the kinetics are hyperbolic with respect to Ru5P. The maximal velocity, given in micromoles per minute, is estimated from the Michaelis−Menten equation fit to the Ru5P saturation data. [b] The K_I of wild-type PRK for 6-phosphogluconate was reported by Runquist et al. (*6*). [c] The K_I for 6-phosphogluconate was not determined for S14A or T20A enzymes.

ATP would be compatible with such an observation. However, the inability to make any comparisons for the β signals limits our ability to interpret these NMR observations without some ambiguity. Another possibility is that, while nucleotide is not released from PRK at a rate that could be considered other than "slow exchange" on an NMR time scale, exchange between different conformers of bound nucleotide might occur in the mutant PRK∗Mg^{2+}−ATP complexes. Such a conformer exchange might result in exchange broadening, accounting for the inability to detect the β signal. However, this alternative explanation might lead to the expectation of exchange broadening of signals from either adjacent phosphoryl group; the spectral data for the mutant complexes (Table 2) do not support such an expectation.

Since the biophysical approaches used to study the model PRK∗Mg^{2+}−ATP complex did not indicate clear differences in how the interactions due to T18, S19, or T20 might translate into different levels of catalytic efficiency, a kinetic approach was employed to investigate whether the various P-loop mutants exhibit diverse functional properties under steady-state turnover conditions.

Kinetic Characterization of PRK Mutants. Steady-state kinetic measurements were performed to evaluate both allosteric activation and catalytic properties of the various P-loop mutants. In the context of activation by the positive effector, NADH, all of the mutants retained sensitivity to this activator (as expected on the basis of the demonstration of their ability to bind NADH; Table 1) although the increase in S14A activity was only half of the increment measured for the wild-type enzyme and the other P-loop mutants (Table 3). Evaluation of substrate saturation indicated that elimination of the alcohol side chains produced only modest inflation in $S_{1/2\ ATP}$, with the largest effects (<8-fold) observed for T18A and S19A. All mutant PRKs retain the sigmoidal ATP binding property exhibited by the wild-type enzyme. In the context of Ru5P saturation, S14A and T20A show only modest inflation of K_m (<7-fold) while larger effects (Table 3) are observed for T18A (45-fold) and S19A (30-fold). In the case of S19A, saturation by Ru5P exhibits a slightly sigmoidal pattern. The extent to which the inflation of $K_{m\ Ru5P}$ reflects altered binding of this substrate can be evaluated by comparison of changes in K_I for the competitive inhibitor, 6-phosphogluconate (*6*). Measurement of these K_I values for T18A and S19A (∼0.2 mM; Table 3) indicates negligible changes upon elimination of the alcohol side chain, suggesting that the observation of $K_{m\ Ru5P}$ inflation does not reflect direct participation of these residues in Ru5P binding (*6*). Comparison of V_{max} values for wild-type and mutant PRKs indicates that elimination of the alcohols at T18 and T20 does not have a major impact on catalytic rate. Substitution to replace the alcohol of invariant S14 has a substantial effect (∼40-fold diminution), but such an observation does not qualify this residue as crucial to catalysis. In contrast, elimination of the alcohol from S19 has larger impact (∼500-fold diminution of V_{max}; >15000-fold diminution in V/K_{Ru5P}; Table 3) that suggests more direct involvement of this residue at the active site. Thus, kinetic characterization of these mutants efficiently discriminates between the relative functional importance of S14, T18, S19, and T20.

DISCUSSION

The assertion that all PRK proteins contain an N-terminal region sequence that qualifies as a P-loop seems plausible on the basis of the alignment depicted in Figure 1, although residues 12−19 clearly exhibit deviations from the consensus G-X-X-X-X-G-K-T/S motif (*7*). For example, eukaryotic PRKs contain alanine (not glycine) as the first residue in the motif. The typical lysine residue does not appear as the seventh residue in prokaryotic PRKs. Finally, at the eighth position in the proposed P-loop sequence, no residue is invariant although a side chain alcohol is always contributed by either the serine or threonine found in various PRKs. The third residue in the PRK sequence is invariably serine, while invariant glycines account for the fourth and sixth residues. Any reservations over whether this N-terminal region qualifies as a P-loop are minimized on the basis of the X-ray structure (*3*), which indicates that this stretch of PRK sequence exists as a dynamic loop which maps in the NMP kinase fold at the position where P-loops have typically been reported. The ^{31}P NMR approach proves valuable in addressing this issue more directly. The data (Figure 5, Table 2) for the PRK∗Mg^{2+}−ATP samples prepared using the wild-type enzyme and any of the T18A, S19A, or T20A mutants indicate that modifications at each of several positions in the P-loop affect the environment of bound ATP.

Recognition of the P-loop motif in an NMP kinase fold protein does not a priori guarantee straightforward assignment of a M^{2+}−ATP ligand. In the well-documented cases of adenylate kinase (*16*) and UMP kinase (*17*), water molecules rather than amino acid side chains fill those cation liganding positions which are not occupied by the phosphoryl oxygens of the ATP substrate. In such examples, numerous conserved basic residues are closely juxtaposed to ATP, providing an electron sink for the negatively charged nucleotide. Such a situation does not appear to be clearly

applicable to PRK where, in the prokaryotic proteins, the glycine-rich loop does not contain a single basic residue (Figure 1). In those phosphotransferases where a P-loop side chain has been implicated in cation liganding (*14*, *15*), a threonine or serine residue mapping at position 8 in the motif has been identified; the serine found in most PRKs can plausibly be invoked to support such a function. Such an observation argues against extrapolating the adenylate kinase model for $M^{2+}-$ATP liganding to PRK. The argument is reinforced by the hypothesis that residue E131 represents a Walker B carboxyl. While some features of the extended consensus sequence proposed by Walker (*8*) are not apparent in PRK alignments, it is clear that PRK's invariant residues 131−135 (EGLH) are always preceded by the four hydrophobic residues that are a key element of the motif. This observation has prompted the assertion that E131 qualifies as a Walker B carboxyl and functions as a $M^{2+}-$ATP ligand (*2*). This sequence motif-based hypothesis is supported by E131's adjacent positioning not only to the P-loop in PRK's active site (*3*) but also to D42, which is proposed to function as the general base catalyst (*25*) that deprotonates the C1 alcohol of Ru5P to facilitate attack on the γ-phosphoryl of ATP.

If the adenylate kinase/UMP kinase models (multiple water ligands to $M^{2+}-$ATP) are to be discounted and E131 proposed as one of two amino acid side chain derived ligands, two issues arise and are addressed in this report. Does the P-loop contribute the second Mg−ATP ligand? If so, will only one of the four alcohol side chains (S14, T18, S19, T20) effectively function as the second Mg−ATP ligand? While modest inflation of substrate saturation parameters for ATP and, more pronouncedly, for Ru5P is observed for both T18A and S19A mutants (Table 3), kinetic characterization of the various P-loop variants indicates that marked (500-fold) impairment of catalytic efficiency only occurs for S19A. Thus, the kinetic characterization results not only suggest that S19 qualifies for consideration as the second $M^{2+}-$ATP ligand but also indicate that (despite flexibility in the dynamic loop) S14, T18, and T20 do not function well as surrogate ligands.

The magnitude of changes in kinetic parameters for PRK mutants should correlate with the proposed function of substituted side chains. In the context of k_{cat} perturbations, part of the ∼40-fold k_{cat} effect measured for substitution of invariant S14 may be attributed to diminished efficiency of NADH activation observed for this mutant. Similarly, mutation of R31, situated within the helix immediately downstream of PRK's P-loop, has also been demonstrated to perturb allosteric activation (*4*). In contrast with the modest k_{cat} effect observed for S14A, the diminution in k_{cat} observed for S19A (500-fold) suggests that this residue is the better candidate for assignment as a ligand to $M^{2+}-$ATP (Figure 6).

Substitution of a protein ligand to $Mg^{2+}-$ATP results in k_{cat} effects for phosphotransferases that exhibit a variety of protein folds [e.g., phosphofructokinase (*30*), fructose-6-phosphate 2-kinase (*31*), mevalonate kinase (*32*)]. Mutagenesis of a side chain that functions solely to ligate $M^{2+}-$ATP typically results in a diminution of k_{cat} by approximately 2 orders of magnitude. In cases where larger effects ($>10^3$-fold) have been observed (*33*, *34*), the side chains have been proposed to have the additional role of facilitating attack on

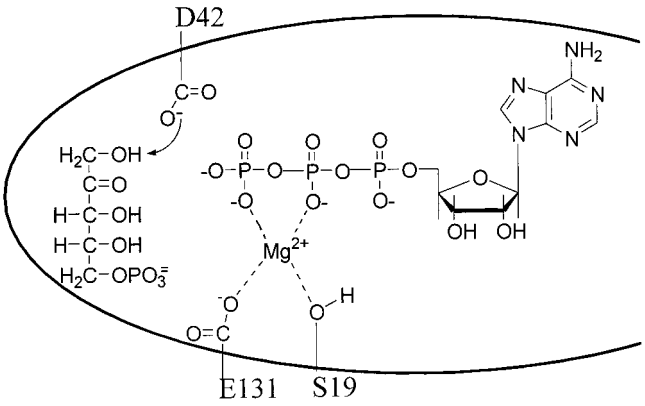

FIGURE 6: Schematic view of the phosphoribulokinase active site. Selected residues mapped to the active site and implicated in the phosphoryl-transfer process on the basis of work presented in this or earlier reports are indicated. Asp-42 has been implicated as a general base catalyst, facilitating deprotonation of the C1 hydroxyl of Ru5P prior to attack on the γ-phosphoryl group of ATP. Glu-131 and Ser-19 are indicated as ligands to the cation of the $Mg^{2+}-$ATP substrate.

ATP's γ-phosphoryl group by hydrogen bonding to the phosphoryl oxygens and optimizing the angle of attack. While the consequences of S19 replacement are not so large, a minor orientation contribution for S19 cannot, at present, be dismissed. Structural information on a PRK∗metal−nucleotide complex in which the P-loop is less dynamic may ultimately be required to evaluate such possibilities.

The inflation of K_m for the phosphoryl acceptor observed with S19A does not necessarily imply an additional Ru5P binding function, since altered catalytic (rather than binding) terms may contribute to the effect. $K_{m\ acceptor}$ inflation has also been documented to be a consequence of mutagenic elimination of $M^{2+}-$ATP ligands in several other phosphotransferases [e.g., phosphofructokinase (*30*), fructose-6-phosphate 2-kinase (*31*), and mevalonate kinase (*32*)]. In contrast to observations made for PRK's H45, R49, and K165 mutants (*6*) which exhibit $K_{m\ Ru5P}$ inflation that parallels $K_{I\ 6PG}$ inflation (implicating these residues in acceptor site binding), S19A exhibits $K_{m\ Ru5P}$ inflation without a significant effect on $K_{I\ 6PG}$. Thus, the data do not suggest direct involvement of S19 with the phosphoryl acceptor, Ru5P. The data for this P-loop residue are most straightforwardly interpreted as indicating an interaction with the ATP site. However, given the lack of direct evidence on cation liganding from EPR experiments and the indirect nature of ^{31}P NMR observations on ATP's phosphoryl groups, a hydrogen-bonding interaction remains a possible alternative explanation so any precise assignment for S19 must be viewed as provisional.

Nonetheless, a function for S19, the eighth residue of PRK's P-loop motif, in liganding to the cation of the $M^{2+}-$ATP substrate clearly represents the most probable assignment. Such a function remains well precedented and is certainly compatible with all experimental data.

ACKNOWLEDGMENT

EPR measurements were performed using the facilities of the National Biomedical ESR Center (NIH RR01008).

REFERENCES

1. Hurwitz, J., Weissbach, A., Horecker, B. L., and Smyrniotis, P. Z. (1956) *J. Biol. Chem. 218*, 769−783.
2. Miziorko, H. M. (2000) *Adv. Enzymol. Relat. Areas Mol. Biol. 74*, 95−128.
3. Harrison, D. H. T., Runquist, J. A., Holub, A., and Miziorko, H. M. (1998) *Biochemistry 37*, 5074−5085.
4. Kung, G., Runquist, J. A., Miziorko, H. M., and Harrison, D. H. T. (1999) *Biochemistry 38*, 15157−15165.
5. Sandbaken, M. G., Runquist, J. A., Barbieri, J. T. and Miziorko, H. M. (1992) *Biochemistry 31*, 3715−3719.
6. Runquist, J. A., Harrison, D. H. T., and Miziorko, H. M. (1999) *Biochemistry 38*, 13999−14005.
7. Saraste, M., Sibbald, P. R., and Wittinghofer, A. (1990) *Trends Biochem. Sci. 15*, 430−434.
8. Walker, J. E., Saraste, M., Runswick, M. J., and Gay, N. J. (1982) *EMBO J. 1*, 945−951.
9. Porter, M. A., and Hartman, F. C. (1986) *Biochemistry 25*, 7314−7318.
10. Porter, M. A., Stringer, C. D., and Hartman, F. C. (1988) *J. Biol. Chem. 263*, 123−129.
11. Omnaas, J., Porter, M. A., and Hartman, F. C. (1985) *Arch. Biochem. Biophys. 236*, 646−653.
12. Krieger, T. J., and Miziorko, H. M. (1986) *Biochemistry 25*, 3496−3501.
13. Krieger, T. J., Mende-Mueller, L., and Miziorko, H. M. (1987) *Biochim. Biophys. Acta 915*, 112−119.
14. Krell, T., Coggins, J. R., and Lapthorn, A. J. (1998) *J. Mol. Biol. 278*, 983−997.
15. Hasemann, C. A., Istvan, E. S., Uyeda, K., and Deisenhofer, J. (1996) *Structure 4*, 1017−1029.
16. Abele, U., and Schulz, G. E. (1995) *Protein Sci. 4*, 1262−1271.
17. Schlichting, I., and Reinstein, J. (1997) *Biochemistry 36*, 9290−9296.
18. Runquist, J. A., and Miziorko, H. M. (2000) *Biochemistry 39*, 1550.
19. Runquist, J. A., Narasimhan, C., Wolff, C. E., Koteiche, H. A., and Miziorko, H. M. (1996) *Biochemistry 35*, 15049−15056.
20. Bagshaw, C. R., and Harris, D. A. (1988) in *Spectrophotometry and Spectrofluorimetry* (Harris, D. A., and Bashford, C. L., Eds.) pp 91−113, IRL Press, Washington, DC.
21. Davenport, D. (1971) in *Fluorescence Spectroscopy* (Pesce, A. J., Rosen, C. G., and Pasby, T. L., Eds.) pp 203−240, Marcel Dekker, New York.
22. Paulsen, J. M., and Lane, M. D. (1966) *Biochemistry 5*, 2350−2357.
23. Marquardt, D. W. (1963) *SIAM J. Appl. Math. 2*, 431−441.
24. Smith, C., and Rayment, I. (1996) *Biophys. J. 70*, 1590−1602.
25. Charlier, H. A., Runquist, J. A. and Miziorko, H. M. (1994) *Biochemistry 33*, 9343−9350.
26. Ho, S. N., Hunt, H. D., Horton, R. M., Pullen, J. K., and Pease, L. R. (1989) *Gene 77*, 51−59.
27. Miziorko, H. M., and Sealy, R. C. (1984) *Biochemistry 23*, 479−485.
28. Reed, G. H., and Ray, W. S. (1971) *Biochemistry 10*, 3190−3197.
29. Brauer, M., and Sykes, B. D. (1987) in *Phosphorus NMR in Biology* (Burt, C. T., Ed.) pp 153−181, CRC Press, Boca Raton, FL.
30. Berger, S. A., and Evans, P. R. (1992) *Biochemistry 31*, 9237−9242.
31. Uyeda, K., Wang, X. L., Mizuguchi, H., Li, Y., Nguyen, C., and Hasemann, C. A. (1997) *J. Biol. Chem. 272*, 7867−7872.
32. Potter, D., and Miziorko, H. M. (1997) *J. Biol. Chem. 272*, 25449−25454.
33. Vertommen, D., Bertrand, L., Sonntag, B., DiPietro, A., Loucks, M. P., Vidal, H., Hue, L., and Rider, M. H. (1996) *J. Biol. Chem. 271*, 17875−17880.
34. Cho, Y. K., Rios, S. L., Kim, J. J. P., and Miziorko, H. M. (2001) *J. Biol. Chem. 276*, 12573−12578.

BI010778C